Thermochimica Acta, 189 (1991) 283–296
Elsevier Science Publishers B.V., Amsterdam

Thermal behaviour of 3-nitro-1,2,4-triazol-5-one and its salts

Xie Yi [1], Hu Rongzu [1], Wang Xiyou, Fu Xiayun and Zhu Chunhua

Xian Modern Chemistry Research Institute, Xian, 710061 Shaanxi (People's Republic of China)

(Received 20 February 1991)

Abstract

3-Nitro-1,2,4-triazol-5-one (NTO) is a new explosive with high energy and low sensitivity, whose salt derivatives are also very useful. Under linear temperature increase conditions, the mechanisms and kinetic parameters of thermal decomposition of NTO and $M \cdot (NTO)_m \cdot nH_2O$ ($M = Cu$, $m = 2$, $n = 4$; $M = Pb$, $H_3NCH_2CH_2NH_3$, $m = 2$, $n = 0$; $M = K$, NH_4, $m = 1$, $n = 1$) are obtained by TG, DSC, IR and X-ray diffraction. The thermal decomposition processes of $Cu \cdot (NTO)_2 \cdot 4H_2O$ and $K \cdot NTO \cdot H_2O$ can be divided into three stages: dehydration, ring breaking, and forming metal oxide. However the thermal decomposition process of $Pb \cdot (NTO)_2$ has only two stages because there is no crystal water. The decomposition process of $NH_4 \cdot NTO \cdot H_2O$ has three stages as well, but they are dehydration, deamination, and decomposition reaction of NTO, which is formed in the second stage. However, if the sample is sealed in a closed stainless steel cell, or the ammonia produced in the second stage does not escape as fast as it is produced, the gaseous ammonia will catalyse the decomposition of NTO.

INTRODUCTION

Nowadays, in the research area of synthesis of explosives, high quality simple compounds are sought with high energy, high density, heat-resistance, and low sensitivity. It has been shown that the high explosives commonly applied, including RDX, TNT, HMX, etc., have a critical shortcoming of high sensitivity to impact and shock, which implies that it is necessary to look for a new explosive with high energy and lower sensitivity. Fortunately, 3-nitro-1,2,4-triazol-5-one (NTO) is just such an explosive, since its energy is as high as that of RDX, while its sensitivity is close to that of TATB, which has attracted many researchers' attentions all over the world. The salts of NTO present special characteristics, and will be used in various fields.

As do other high nitrogen compounds, NTO has the advantages of high nitrogen, high density, low sensitivity, and high thermal enthalpy [1], which

[1] Authors to whom correspondence should be addressed.

0040-6031/91/$03.50

are determined by the special structure of nitrogen atom in its molecule. Firstly, the bond lengths C–N (1.352 Å), N–N (1.020 Å) and N=N (1.094 Å) are shorter than C–C (1.530 Å) and C=C (1.330 Å). Hence, NTO has less mole volume and higher density ($d = 1.93$ g cm^{-3}). Secondly, the bond angles of the NTO ring are relatively homogeneous. The bond angle C–N=C ($\approx 102°$) is less than the C–C=C bond angle ($\approx 124°$) and approaches the average bond angle of five-membered ring compounds (108°); hence the tensile force of the ring of NTO is relatively weak. The isolated double electrons on the nitrogen atom join the conjugation, which results in the aromaticity of the ring being enhanced, i.e. the thermal stability is increased. Thirdly, owing to the existence of intermolecular hydrogen bonds, the melting point of NTO is greatly increased and is higher than its decomposition temperature. In addition, it is important that NTO can easily be synthesized with inexpensive starting materials. Hence, as a new explosive, NTO has good prospects in the near future. Also the salts of NTO will be exploitable. Seldom, however, have their mechanisms and kinetic parameters of thermal decomposition been reported. In this paper, we report studies on their thermal behaviour under non-isothermal conditions by means of TG, DSC, IR, and X-ray diffraction; study of their rules of change at elevated temperature conditions, both in theory and practice, is very significant. Also, by means of ^{13}C NMR, we have determined the site from which the hydrogen of NTO leaves.

EXPERIMENTAL

Materials

NTO and its ethylenediammonium salt (ENTO), ammonium salt (ANTO), and potassium salt (KNTO) were prepared according to reported methods [2,3]. The copper salt (CuNTO) and lead salt (PbNTO) of NTO were prepared in our Institute. Some of their properties are shown in Table 1; their structures were determined by elemental analysis, IR, NMR, and X-ray diffraction.

TABLE 1

Structure and properties of the sample

Sample	Molecular formula	Mol. mass	Crystal colour
NTO	$C_2H_2N_4O_3$	130.06	White
ENTO	$C_6H_{12}N_{10}O_6$	320.22	Light yellow
CuNTO	$C_4H_2N_8O_6 \cdot Cu \cdot 4H_2O$	393.65	Green
KNTO	$C_2HN_4O_3 \cdot K \cdot H_2O$	186.17	Light yellow
PbNTO	$C_4H_2N_8O_6 \cdot Pb$	465.31	Yellow
ANTO	$C_2H_5N_5O_3 \cdot H_2O$	165.09	Light yellow

Experimental apparatus and conditions

In the present experiment, the thermal decomposition processes were studied using TG technique on a Delta Series TGA7 (Perkin Elmer Co., USA). The conditions of TG were as follows: sample mass, about 1 mg; heating rate, 10 °C min^{-1}; atmosphere, flowing N_2/O_2 mixture (with a ratio in air). The kinetic parameters of thermal decomposition have been determined from differential scanning calorimetry (DSC) measurements using a CDR-1 differential scanning calorimeter (Shanghai Tianping Instrumental Factory, China) with a cell of aluminium (diameter 5 mm × 3 mm), whose side is rolled up, and a sealed cell of stainless steel (diameter 5 mm × 2.85 mm) [4]. The conditions of DSC were as follows: sample mass, about 1 mg; heating rates, 1, 2, 5, 10 and 20 °C min^{-1}; sensitivities, ±10.46, ±20.92, ±41.84 mJ s^{-1}; atmosphere, static air; reference sample, α-Al_2O_3; thermocouple plate, Ni/Cr–Ni/Si. The intermediates in coacervate phase were analysed using JDX-752 model X-ray (Nippon Elec. Co.) and 60 SXR-FTIR spectra (Nicolet Co., USA). The hydrogen leaving NTO salt was determined by FX-90QNMR (Nippon Elec. Co.).

RESULTS AND DISCUSSION

Determination of the site from which the hydrogen leaves NTO molecule in NTO salts

The ^{13}C NMR spectra of NTO and its salts are shown in Fig. 1. Comparing NTO with its salts, we find that the chemical shift of the two carbon atoms of NTO salts is to the low field. Because of paramagnetism, the ^{13}C NMR spectrum of CuNTO is not observed. From Table 2, we find that before and after the salts form, the chemical shift changes of the two carbon atoms of the NTO ring are nearly the same, which indicates that the attraction is equal to the two carbon atoms. According to this result, the site from which the hydrogen atom leaves is determined to be at position N4 between the two carbon atoms (see Fig. 2).

Thermal behaviour of NTO and its salts

Typical TG and DSC curves of NTO and its salts under the conditions described above are shown in Fig. 3. Mass losses (%) with temperature under non-isothermal conditions are shown in Table 3. It can be seen from Fig. 3 that under our conditions, the thermal decomposition processes of NTO and ENTO show only one stage on TG curves. NTO decomposes from 205 to 330 °C and ENTO from 178 to 320 °C. A few residues in coacervate phase will be oxidized at high temperature. Both NTO and ENTO have only one sharp exothermic peak on DSC curves. Under the same conditions, the

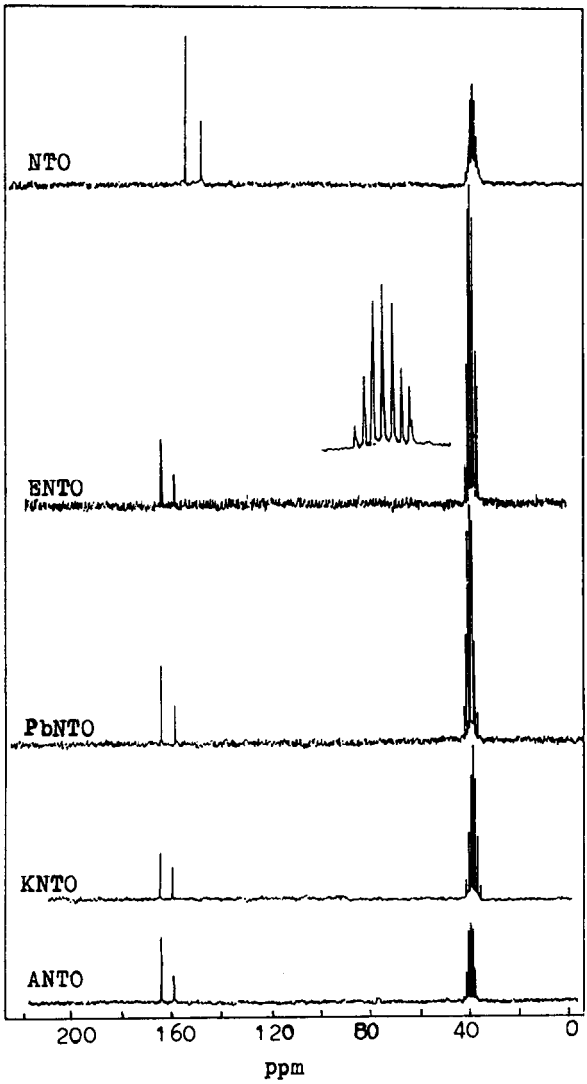

Fig. 1. ^{13}C NMR spectra of NTO and its salts.

TABLE 2

Data of ^{13}C NMR spectra for NTO and its salts

Sample	Solvent	Chemical shift (ppm)	
		$=C-NO_2$	$=C=O$
NTO	$CDCl_3$	148.13	154.70
ENTO	DMSO-d_6	158.80	164.07
PbNTO	DMSO-d_6	159.19	164.52
KNTO	$CDCl_3$	159.97	165.17
ANTO	DMSO-d_6	159.65	164.85

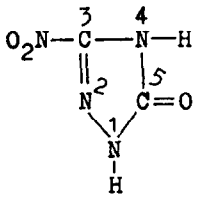

Fig. 2. Structure of the NTO ring.

thermal decomposition processes of the metallic salts of NTO (CuNTO and KNTO) can be divided into three stages: dehydration, ring breaking, and metal oxide formation. The thermal decomposition of PbNTO has only the

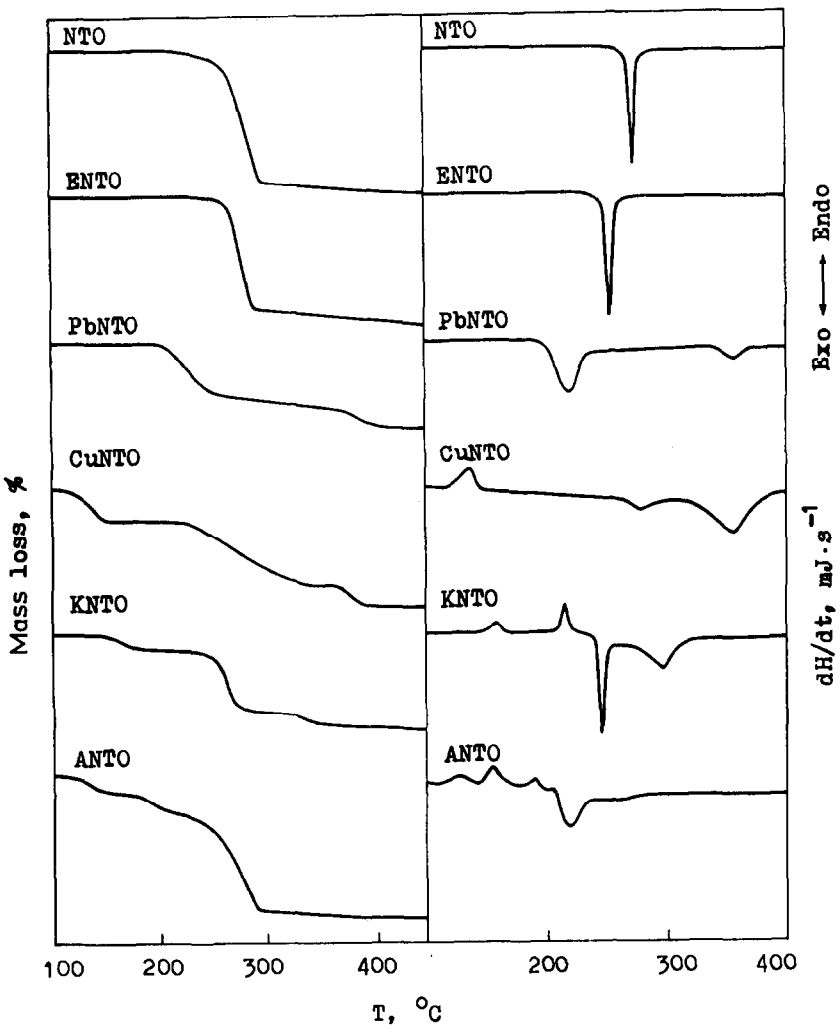

Fig. 3. Typical TG and DSC curves of NTO and its salts.

TABLE 3

Data for the thermal decomposition of NTO and its salts

Compound and decomposition stage	Temperature range (°C)		Mass loss (%)	
	TG	DTG	Obs.	Calc.
NTO  → residues in coacervate phase	205–330	205–294–330	94.9	100
ENTO 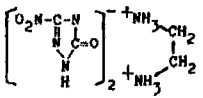 → residues in coacervate phase	178–320	178–282–320	80.8	100
ANTO 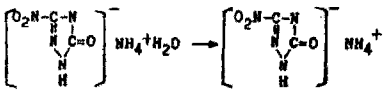	114–160	114–151–160	11.2	10.9
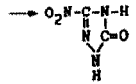	160–204	160–178–204	10.4	10.3
→ residues in coacervate phase	204–323	204–282–323	75.9/97.5	78.8/100
KNTO 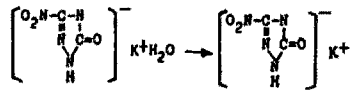	148–219	148–177–219	9.1	9.7
→ intermediates of coacervate phase	219–309	219–275–309	39.5	
→ KO_2	309–378	309–323–378	10.2/58.8	52.2/61.9
CuNTO 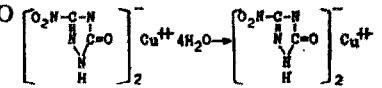	97–167	97–136–167	18.3	18.3
→ intermediates of coacervate phase	167–337	167–247–337	48.5	50.1
→ CuO (crystals)	337–426	337–365–426	12.3/79.1	11.2/79.6
PbNTO 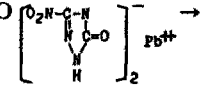 → intermediate of coacervate phase	188–344	188–234–344	41.4	42.6
→ PbO (red crystals)	344–433	344–388–433	15.9/57.3	9.5/52.1

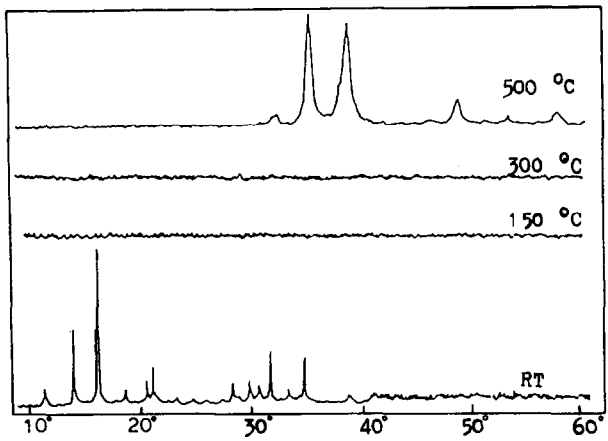

Fig. 4. X-Ray diffraction spectra of CuNTO and its decomposition products.

two latter stages because it does not contain crystal water. It can be seen from Fig. 3 and Table 3 that the first stage of thermal decomposition of CuNTO and KNTO is connected with their dehydration processes in the temperature ranges 97–167 °C for CuNTO and 148–219 °C for KNTO. The mass losses of 18.3% and 9.1% are also in good agreement with the respective calculated values of 18.3% for CuNTO and 9.7% for KNTO. The X-ray diffraction spectrum shows that in the first stage of CuNTO decomposition it becomes a noncrystalline compound (see Fig. 4), but its IR spectrum does not clearly change (see Fig. 5) due to the characteristic absorption peaks of –CO–N · M (M = Cu, K, etc.) coinciding with the peak of H_2O in the bond (2800–3300 cm^{-1}); after dehydration, the dehydrated KNTO easily absorbs water again as soon as it is exposed to the air at room temperature, and so does not present the IR and X-ray diffraction spectra of dehydrated KNTO. In the second stage, the thermal decomposition mechanisms of CuNTO and KNTO are similar to that of the first stage of exothermic decomposition for PbNTO. They decompose in the temperature ranges 167–337 °C for CuNTO, 219–309 °C for KNTO, and 188–344 °C for PbNTO. Mass loss is 48.5% for CuNTO, 39.5% for KNTO, and 41.4% for PbNTO. The results obtained from the IR spectra of CuNTO and PbNTO (shown in Figs. 5 and 6) indicate that characteristic absorption peaks of $-NO_2$ and –CO–N · M (M = Cu, Pb) disappear at 1524, 1311 and 2800–3350 cm^{-1} for CuNTO and at 1513, 1310 and 2800–3300 cm^{-1} for PbNTO. In addition, the characteristic absorption peak of N=C=N appears at 2173 cm^{-1} for the residues of CuNTO and 2145 cm^{-1} for those of PbNTO. The X-ray diffraction spectra show that both the residues are noncrystalline compounds (shown in Figs. 4 and 7). The results indicate that denitrification of NTO and its salts is not an independent process, because ring breaking is accompanied by denitrification, after which the 1,2,4-triazol-5-one (TO) ring can no longer be found. The residues are supposed to

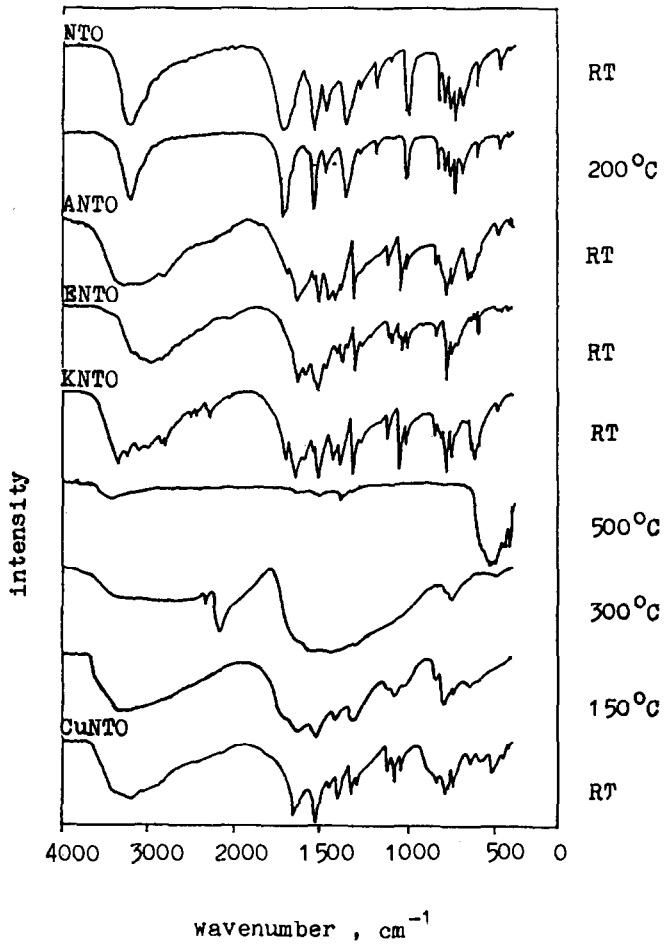

Fig. 5. IR spectra of NTO and its salts, and their decomposition products.

be a mixture including carbonate; their calculated mass losses of 50.1% for CuNTO and 42.6% for PbNTO are in agreement with the experimental values, and in the IR spectra of the residues there are characteristic absorption peaks of $CuCO_3$ and $PbCO_3$ at 1460 cm^{-1}. In the third stage, the residues formed in the second stage further turn into CuO (crystal) and similarly that formed in the first stage for PbNTO turns into PbO (red crystal).

The values of the apparent activation energy, the preexponential constant and the linear correlation coefficient obtained by Kissinger's method and Ozawa's method are listed in Table 4. Comparing those values, the order of the apparent activation energies is as follows: NTO $\gg$ PbNTO > ENTO > KNTO > CuNTO. In fact, NTO is the most stable compound.

It is found that ANTO is a very special compound. Under the condition of flowing air, its thermal decomposition process can be divided into three

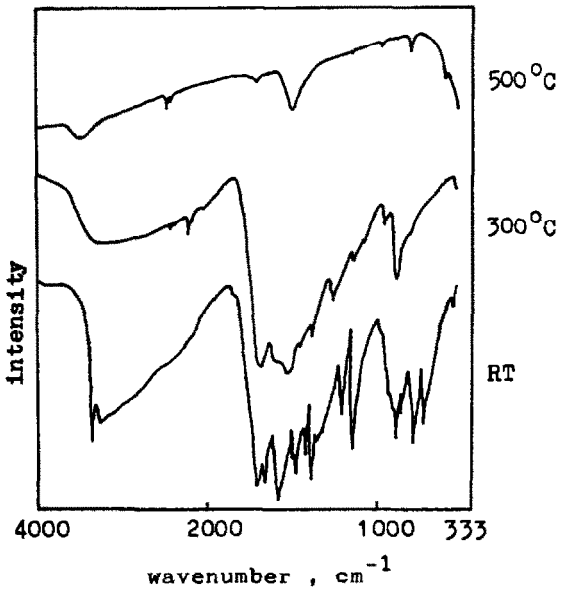

Fig. 6. IR spectra of PbNTO and its decomposition products.

stages. The first stage is its dehydration in the temperature range 114–160 °C. Mass loss of 11.2% is in fair agreement with the calculated value of 10.9%. In the second stage, it is connected with the deamination process in the temperature range 160–204 °C. Mass loss of 10.4% is also in fair agreement with the calculated value of 10.3%. If the sample is taken out at 204 °C and quickly cooled to room temperature, its IR and X-ray diffraction spectra are very similar to those of NTO (see Figs. 5 and 8), which indicates that under the above-mentioned conditions, NTO is formed in the decomposition

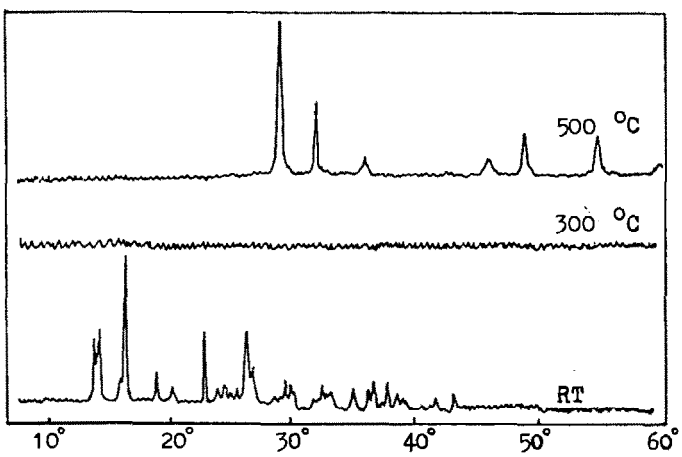

Fig. 7. X-ray diffraction spectra of PbNTO and its decomposition products.

TABLE 4

Calculated values of the kinetic parameters for the exothermic decomposition for NTO and its salts [a]

Sample	Φ (°C min^{-1})	T_m (°C)		E (kJ mol^{-1})				log A_1 (s^{-1})	log A_2 (s^{-1})	r	
		T_{m1}	T_{m2}	E_{k1}	E_{k2}	E_{o1}	E_{o2}			r_{k1}/r_{o1}	r_{k2}/r_{o2}
NTO	1.046	265.5		520.3		503.4		48.1		0.9868/0.9872	
	2.004	267.3									
	5.150	270.5									
	10.05	275.5									
	21.06	278.8									
ENTO	1.045	230.8		214.1		211.8		19.4		0.9967/0.9969	
	1.969	238.5									
	5.071	248.5									
	10.95	254.8									
	20.60	261.0									
PbNTO	0.9891	205.5	323.5	242.3	176.7	237.8	177.6	23.7	12.5	0.9966/0.9968	0.9984/0.9986
	2.027	211.5	332.5								
	4.943	217.8	349.8								
	10.33	222.8	362.2								
	19.87	230.3	373.8								
CuNTO	1.005	241.5	292.8	115.5	87.1	118.3	92.4	8.12	6.98	0.9981/0.9985	0.9976/0.9845
	2.025	253.5	298.3								
	5.114	268.8	325.8								
	10.19	285.3	352.8								
	20.35	300.8	382.2								
KNTO	0.9897	230.0	257.3	192.4	118.0	188.8	121.0	17.1	8.7	0.9976/0.9982	0.9834/0.9857
	2.025	239.8	260.3								
	5.295	249.8	285.3								
	10.47	257.3	301.5								
	21.84	265.0	313.3								

[a] Φ, Heating rate; T_m, maximum peak temperature; r, linear correlation coefficient; E, apparent activation energy; A, pre-exponential constant; subscript k, data obtained by Kissinger's method; subscript o, data obtained by Ozawa's method; subscript 1, first exothermic decomposition peak; subscript 2, second exothermic decomposition peak.

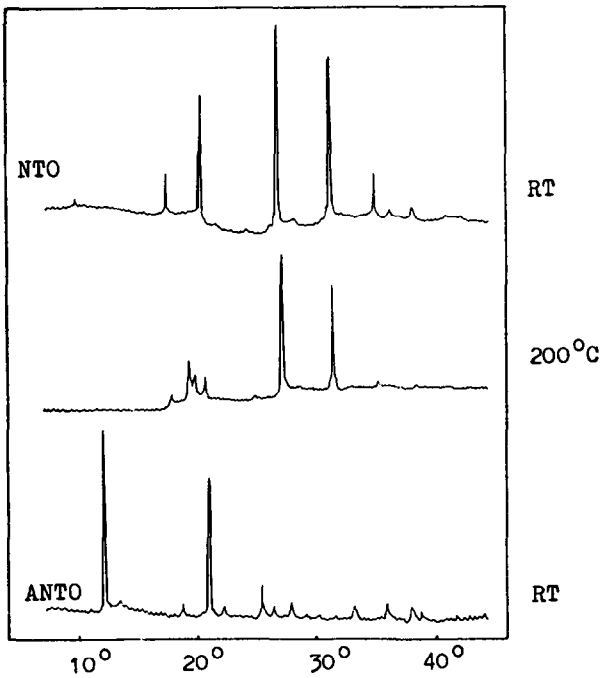

Fig. 8. X-Ray diffraction spectra of NTO, ANTO and the decomposition product of ANTO.

process of ANTO in the second stage. In the third stage, the compound formed in the second stage continues to decompose as does NTO in the temperature range 204–323°C. Mass loss of 75.9% is also in agreement with the calculated value of 78.8%.

However, if we use static air instead of flowing air, the result will be different. Under static air conditions and heating rates of 1 and 2°C min^{-1}, there is a sharp exothermic peak after the two endothermic peaks in the DSC curves. The temperatures at which the exothermic peaks appear are 262.8 and 262.5°C, respectively; these are close to the temperature of decomposition peak of NTO. Under the condition of static air, and heating rates of 5, 10 and 20°C min^{-1}, the exothermic peaks are shifted downwards very much. They appear at 211.5, 221.3 and 236.5°C, respectively (see Fig. 9), which represents shifts 23–58°C downwards. Therefore, it is clear that the mechanism of thermal decomposition in the third stage of ANTO is different from that of single NTO explosive under high heating rate conditions.

For exploring the mechanism of thermal decomposition of ANTO, we used a sealed cell of stainless steel instead of a non-sealed cell of aluminium to run DSC experiments under the same conditions of static air and heating rates of 2, 5 and 10°C min^{-1}, the results of which are shown in Fig. 10. Comparing Fig. 9 with Fig. 10, it can be seen that the exothermic peak of ANTO under a heating rate of 2°C min^{-1} shifts about 44°C downwards,

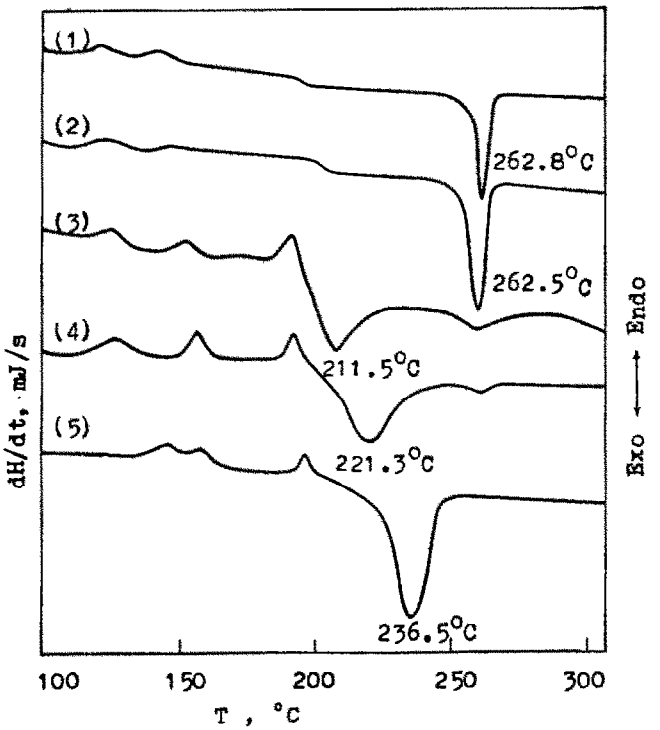

Fig. 9. DSC curves of ANTO with nonsealed cell. Heating rates, (1) 1°C min^{-1}, (2) 2°C min^{-1}, (3) 5°C min^{-1}, (4) 10°C min^{-1}, (5) 20°C min^{-1}.

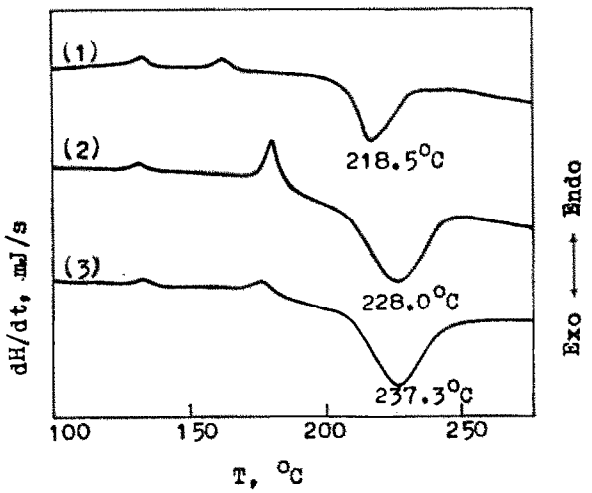

Fig. 10. DSC curves of ANTO with sealed cell of stainless steel. (1) 2°C min^{-1}; (2) 5°C min^{-1}; (3) 10°C min^{-1}.

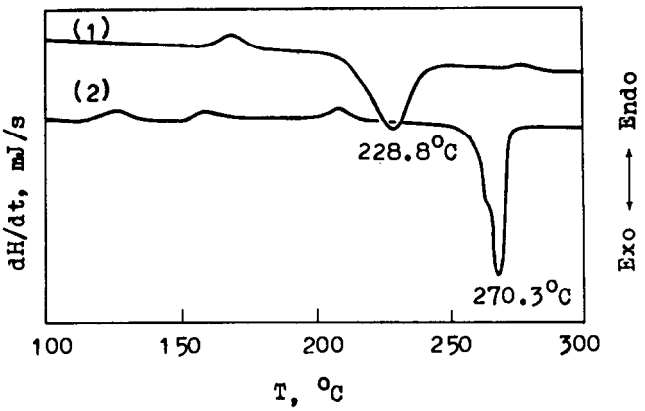

Fig. 11. DSC curves of NTO/ANTO mixture (the mass ratio is 1:1) at a heating rate of 10 °C min^{-1}. (1) Obtained by sealed cell; (2) obtained by non-sealed cell.

appearing at 218.5 °C, but those under the heating rates of 5 and 10 °C min^{-1} shift about 16 °C upwards, appearing at 228.0 and 237.3 °C, all of which are much lower than 275 °C. From the above it is established that the excess gaseous ammonia produced in the second stage, which does not escape from the cell, makes the decomposition reaction of NTO take place at a lower temperature, i.e. there is an autocatalytic reaction during the thermal decomposition of ANTO.

To verify this result, we made a comparative DSC experiment using a mixture of NTO and ANTO with a 1:1 mass ratio as sampled under two conditions: one experiment was carried out with a sealed cell of stainless steel and heating rate of 10 °C min^{-1}, and the other with a nonsealed cell of aluminium and the same heating rate (results are shown in Fig. 11). From Fig. 11, it can be seen that the DSC curve of the sample in a nonsealed cell shows the same temperature of exothermic peak as NTO, but that in a sealed cell of stainless steel shows an exothermic peak at 228.8 °C, which shifts about 40 °C downwards. Thus we can conclude that the gaseous ammonia catalyzes the decomposition reaction of NTO, but ANTO and its intermediate coacervate phase does not.

CONCLUSIONS

By means of the ^{13}C NMR technique, the site from which the hydrogen leaves NTO salt in the molecules of NTO is determined to be the N4 atom.

On the basis of experimental and calculated results, the thermal decomposition mechanisms of NTO and its salts under air can be expressed by the schemes shown in Table 3.

Gaseous ammonia catalyzes the decomposition reaction of NTO, and the thermal decomposition of ANTO is an autocatalytic reaction.

ACKNOWLEDGEMENTS

We express our thanks to Professor Chang Mingnan, Professor Li Fuping and Lecturers Fan Tao, Liang Yanjun, Zhu Lihua, and Wang Yuan for their help in this work.

REFFERENCES

1 K.Y. Lee, L.B. Chapman, and M.D. Coburn, J. Energetic Mater., 5 (1987) 27.
2 D.T. Cromer, J.H. Hall, K.-Y. Lee and R.R. Ryan, Acta Crystallogr., Sect. C, 44 (1988) 1144–1147.
3 G.I. Chipen, R.P. Bokalders and V.I. Grinstein, Khim Geterotsikl. Soedin., 2 (1) (1966) 110.
4 Hu Rongzu, Yang Zhengquan and Liang Yanjun, Thermochim. Acta, 123 (1988) 135.